



A simplified coupled thermo-mechanical model for the transient analysis of temperature-sensitive hydrogels



Zhiwei Ding^{a,b}, William Toh^c, Jianying Hu^d, Zishun Liu^{d,*}, Teng Yong Ng^c

^a Institute of High Performance Computing, 1 Fusionopolis Way, #16-16 Connexis, Singapore 138632, Singapore

^b Department of Material Science and Engineering, Massachusetts Institute of Technology, Cambridge, MA 02142, USA

^c School of Mechanical and Aerospace Engineering, Nanyang Technological University, 50 Nanyang Avenue, Singapore 639798, Singapore

^d International Center for Applied Mechanics, State Key Laboratory for Strength and Vibration of Mechanical Structures, Xi'an Jiaotong University, Xi'an, 710049, People's Republic of China

ARTICLE INFO

Article history:

Received 14 July 2015

Revised 26 February 2016

Available online 22 March 2016

Keywords:

Deformation kinetics

Finite element method

Temperature sensitive hydrogel

Transient swelling

ABSTRACT

The present work investigates the deformation characteristics of a temperature sensitive hydrogel. The state of mechanical and chemical equilibrium is first formulated via a variational approach, upon which a finite element model is developed and implemented through user-defined material subroutine UMAT in the commercial software ABAQUS. We will show that this UMAT implementation allows for more versatility in the imposition of initial conditions over existing models developed using UHYPER subroutine. Furthermore, we propose an approach to simulate the transient swelling process of a temperature sensitive hydrogel. This is achieved through the simultaneous application of three user-defined subroutines, which model the constitutive properties of the gel, as well as the diffusion of solvent molecules within the gel. Several numerical case studies are presented to verify the present model developed with experimental data, as well as to illustrate its capabilities in simulating a wide array of complex gel phenomena, including surface creasing, bifurcation and buckling of gels. Through these numerical examples, we are able to gain deeper insights, and explain some of the new interesting physical phenomena observed in reported experiments.

© 2016 Elsevier Ltd. All rights reserved.

1. Introduction

Crosslinking through covalent bonds, flexible long-chained polymers form a three-dimensional elastomeric gel network which swells after imbibing the solvent. The strong covalent bonds enable the gel structure to maintain its shape, while the polymer network and solvent are aggregated by weak bonds that enable transport. With various functional groups along the polymer chain, a hydrogel could deform in response to different stimuli such as ionic concentration (Lai and Li, 2011), temperature

(Drozdov, 2015), forces, pH values (De and Aluru, 2004; Marcombe et al., 2010), electrical field and light (Toh et al., 2014a). In addition to the stimuli-responsive property, the capability of being large and reversible deformation and biocompatibility assures hydrogel as an attractive material choice in diverse applications. Such applications include sensors, actuators and micro-valves, drug delivery devices and tissue engineering.

These promising applications, together with some interesting phenomena, such as buckling, pattern transformation and surface instabilities have motivated a large number of theoretical and numerical studies on hydrogels. In recent development of nonlinear field theories (Chester and Anand, 2010, 2011; Hong et al., 2010; Hong et al., 2008), it is assumed that gels generally undergo two

* Corresponding author. Tel.: +86 29 82664354.

E-mail address: zishunliu@mail.xjtu.edu.cn, zishunliu@nus.edu.sg (Z. Liu).

modes of deformation. In the first mode, the gel changes its shape rapidly, but maintains a constant volume through the stretching of polymer chains and local rearrangement of solvent molecules. Thus, the gel behaves like an incompressible elastomer and it is often treated as an instantaneous process. The second mode involves long-range transport of small molecules, allowing the gel to swell or shrink. This mode is a slow and size-dependent process.

Numerical methods, such as the finite element method (FEM), are normally adopted to study deformation behaviors of gels. In earlier studies of deformation of gels, most numerical simulation works focus on the equilibrium states (Ding et al., 2013; Hong et al., 2009; Kang and Huang, 2010; Marcombe et al., 2010; Toh et al., 2013; Toh et al., 2014a). For transient problems of gels, different numerical approaches are used to conduct transient analysis of hydrogels. One such approach is using COMSOL MULTIPHYSICS software. Another numerical approach is to develop special purposed user-defined elements using the UEL subroutine in ABAQUS. Chester et al. (2015) formulated an FEM for transient analysis of concurrent large deformation and mass transport in gels using this approach. One other numerical approach is to make use of the similarities in the governing equations between diffusion and heat transfer to simulate mass diffusion as an equivalent heat transfer process. Following this approach, Toh et al. developed and implemented the numerical method to study the transient behavior of polymeric gels (Toh et al., 2013) and pH-sensitive hydrogels (Toh et al., 2014b).

Recently, Ding et al. (2013) modeled the large deformation of temperature-sensitive hydrogels and implemented it through user-subroutine UHYPER in ABAQUS. However, due to the built-in constraints of UHYPER, the usage of UHYPER is limited to isotropic initial conditions (Kang and Huang, 2010). In this present study, we implement the finite element model using a more robust subroutine to study the equilibrium state and highlight its advantage over existing methods through numerical examples.

The deformation kinetics of temperature-sensitive hydrogel consist of polymer chains stretching, diffusion of solvent molecules, and heat transfer process. In the present study, a method to perform transient analysis for swelling of temperature-sensitive hydrogel is formulated and implemented with the combination of several subroutines. Although it is possible to formulate user-defined elements (UEL) for the transient simulation of temperature-sensitive gel swelling (Chester and Anand, 2011), we note that the process of developing a functional UEL requires a substantial amount of effort and the implementation is not straightforward. In our proposed method, the implementation does not involve development of new elements by coupling mass diffusion, heat transfer and deformation in FEM. It is expected that this approach can be employed in a more user-friendly manner.

The paper is organized as follows. In Section 2, we derive governing equations and equilibrium conditions for a gel undergoing inhomogeneous deformation using a variational approach. Adopting an explicit free energy model, constitutive equations and chemical potential of solvent molecular within a gel are derived and discussed in Section 3. Finite element methods for static and tran-

sient analysis are proposed and implemented in Section 4. Section 5 presents numerical examples to verify the correctness and highlight the advantages of our method. To demonstrate the reliability of our method for transient analysis, in Section 6, we compare the simulation results with experimental results and validate the assumption made in Section 4.2. In Section 7, we apply our proposed numerical methodology to explain experimental observations such as substrate-controlled creasing, bifurcation, and buckling of swelling gels. The last section contains our concluding remarks.

2. Governing equations and equilibrium conditions

Here we adopt a variational approach in deriving the governing equations and equilibrium conditions when a gel undergoes isothermal inhomogeneous large deformation. An analogous variational approach was proposed by Kang and Huang (2010). We did not specifically write out the first and second thermodynamic principles like the work of Chester and Anand (2011). The reason is that neither of the two principles is used in the static and transient analysis. Only an isothermal process is considered, as it is well known that thermal equilibrium implies a homogeneous temperature field.

Consider a hydrogel body (reference state) of volume Ω_0 enclosed by a surface Γ_0 as shown in Fig. 1. When the hydrogel is immersed in a solvent of chemical potential $\tilde{\mu}$, solvent molecules can enter or leave the polymeric gel across the surface Γ . In the system, the gel is subjected to a body force b_i and surface traction t_i . In addition, the surface Γ may be mechanically constrained or chemically isolated from the solvent. We regard the dry gel states as the reference state, and the deformation gradient \mathbf{F} is defined as the mapping from the reference state coordinates \mathbf{X} to the current state \mathbf{x} .

$$F_{iK} = \frac{\partial x_i(\mathbf{X})}{\partial X_K} \quad (1)$$

To obtain the equilibrium condition, consider an infinitesimal process where in a short time δt , the displacement field in the reference coordinate is denoted by $\delta \mathbf{x}(\mathbf{X})$ and the work done δH by the environment in the reference coordinates is expressed as

$$\delta H = \int_{\Omega_0} B_i \delta x_i dV_0 + \int_{\Gamma_0} T_i \delta x_i dS_0 + \int_{\Omega_0} \tilde{\mu} \delta C dV_0 \quad (2)$$

where C is the nominal volumetric concentration of the solvent molecules, which is defined as the number of solvent molecules in the current configuration per unit volume in the reference state. dV_0 and dS_0 are the differential volume and area respectively in the reference frame. B_i and T_i are the nominal body force and nominal surface traction, which are defined as the body force in the current state per unit volume in the reference state and surface traction in the current state per unit area in the reference state respectively.

Assuming a general form of the nominal free energy density function $W(\mathbf{F}, C)$ at a certain temperature, the variation of energy of the hydrogel, δU is

$$\delta U = \int_{\Omega_0} \delta W dV_0 = \int_{\Omega_0} \frac{\partial W}{\partial F_{iK}} \delta F_{iK} dV_0 + \int_{\Omega_0} \frac{\partial W}{\partial C} \delta C dV_0 \quad (3)$$

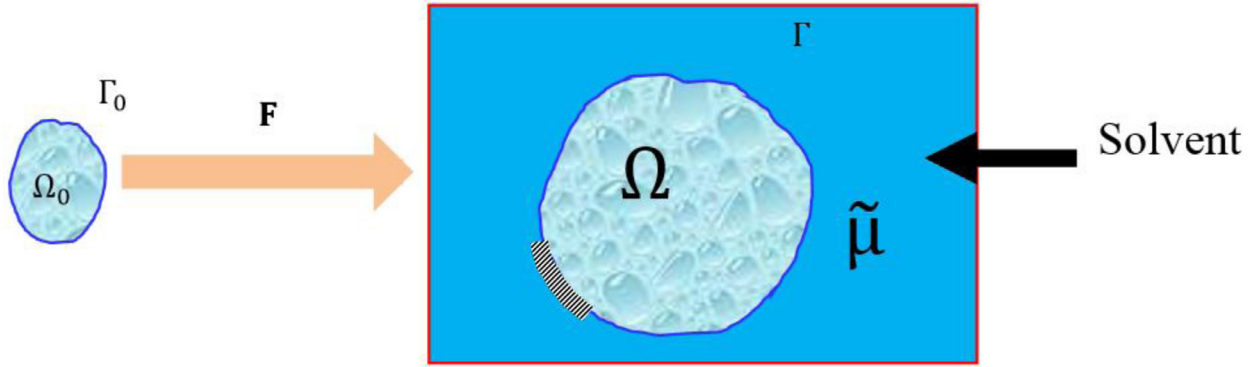


Fig. 1. A dry polymeric gel in reference state when placed in contact with a solvent deforms to current state.

Integrating by parts to evaluate the first term, we get

$$\begin{aligned} \delta U = & \int_{\Omega_0} \frac{\partial}{\partial X_K} \left(\frac{\partial W}{\partial F_{iK}} \delta x_i \right) dV_0 - \int_{\Omega_0} \frac{\partial}{\partial X_K} \left(\frac{\partial W}{\partial F_{iK}} \right) \delta x_i dV_0 \\ & + \int_{\Omega_0} \frac{\partial W}{\partial C} \delta C dV_0 \end{aligned} \quad (4)$$

Applying divergence theorem to the first term of Eq. (4), we obtain

$$\begin{aligned} \delta U = & \int_{\Gamma_0} \frac{\partial W}{\partial F_{iK}} N_K \delta x_i dS_0 - \int_{\Omega_0} \frac{\partial}{\partial X_K} \left(\frac{\partial W}{\partial F_{iK}} \right) \delta x_i dV_0 \\ & + \int_{\Omega_0} \frac{\partial W}{\partial C} \delta C dV_0 \end{aligned} \quad (5)$$

The principle of virtual work requires that

$$\delta U = \delta H \quad (6)$$

Substituting Eqs. (2) and (5) into Eq. (6) yields

$$\begin{aligned} \int_{\Gamma_0} \left(\frac{\partial W}{\partial F_{iK}} N_K - T_i \right) \delta x_i dS_0 - \int_{\Omega_0} \left(\frac{\partial}{\partial X_K} \frac{\partial W}{\partial F_{iK}} + B_i \right) \delta x_i dV_0 \\ + \int_{\Omega_0} \left(\frac{\partial W}{\partial C} - \tilde{\mu} \right) \delta C dV_0 = 0 \end{aligned} \quad (7)$$

Eq. (7) holds for arbitrary changes δx_i and δC and so the quantity in each pair of parentheses vanishes. Thus we arrive at the equilibrium conditions.

$$\frac{\partial}{\partial X_K} \frac{\partial W}{\partial F_{iK}} + B_i = 0 \text{ in } \Omega_0 \quad (8)$$

$$\left(\frac{\partial W}{\partial C} - \tilde{\mu} \right) = 0 \text{ in } \Omega_0 \quad (9)$$

$$\frac{\partial W}{\partial F_{iK}} N_K - T_i = 0 \text{ on } \Gamma_0 \quad (10)$$

The nominal stress S_{iK} may be defined as the work conjugate of the deformation gradient, i.e.

$$S_{iK} = \frac{\partial W}{\partial F_{iK}} \quad (11)$$

In such case, Eqs. (8) and (10) can be interpreted as the conditions for mechanical equilibrium. From Eq. (9), we note that the chemical potential of solvent molecules

inside gel μ can be defined as the work conjugate of the solvent concentration, i.e.

$$\mu = \frac{\partial W}{\partial C} \quad (12)$$

Eqs. (9) and (12) stipulate that the chemical potential of solvent with the gel is homogenous and equal to the chemical potential of the external solvent during the equilibrium state. Although in the transient analysis, the chemical potential is not homogeneous, Eq. (12) has provided a way to evaluate the chemical potential of solvent molecules inside the gel for every elementary volume.

3. Free energy model and constitutive equations

Based on the work of Cai and Suo (2011), the field theory of temperature-sensitive hydrogels is further refined here. Since the crosslink density is typically very low, we assume that the impact of crosslink density on the interaction between the monomers and the solvent molecules is negligible. Hence the Helmholtz Free energy of the hydrogel is considered to consist of (i) the stretching of the network and (ii) the mixing of the polymer and the solvent independently. Therefore, the free energy density of gel can be written as:

$$W = W_{\text{stretch}}(\mathbf{F}) + W_{\text{mix}}(C, T) \quad (13)$$

where W_{stretch} is due to the stretching of the network, and W_{mix} is the energy due to the mixing of the polymers and solvent.

We assume that the individual long polymers and the individual small molecules are incompressible. The condition of molecular incompressibility is expressed as (Hong et al., 2008)

$$\det(\mathbf{F}) = 1 + \nu C \quad (14)$$

The condition of molecular incompressibility can be reinforced as a constraint by adding a term $\Pi[1 + \nu C - \det(\mathbf{F})]$ to the free energy density function, where Π is the Lagrange multiplier, which can also be interpreted as the osmotic pressure as discussed by Hong et al.(2008). The Lagrange multiplier is used so that \mathbf{F} and C can be treated as independent variables, which is consistent with the framework in Section 2. Hence, the

free energy density W takes the form:

$$W = W_{\text{stretch}}(\mathbf{F}) + W_{\text{mix}}(C, T) + \Pi[1 + \nu C - \det(\mathbf{F})] \quad (15)$$

A general expression for Π can be obtained by substituting Eq. (15) into Eq. (12)

$$\Pi = \frac{1}{\nu} \left(\mu - \frac{\partial W_{\text{mix}}}{\partial C} \right) \quad (16)$$

The expression obtained here is consistent with the works of Hong et al. (2008) and Cai and Suo (2012).

The free energy due to the stretching of a network of polymer is taken to be (Flory, 1953)

$$W_{\text{stretch}}(\mathbf{F}) = \frac{1}{2} NkT [F_{ik}F_{ik} - 3 - 2 \ln(\det \mathbf{F})] \quad (17)$$

where N is the number of polymer chains per unit dry volume, kT the temperature in terms of energy, and ν the volume per water molecule

The energy of mixing of the long polymer with the solvent is taken to be

$$W_{\text{mix}}(C, T) = kT \left[C \ln \left(\frac{\nu C}{1 + \nu C} \right) + \frac{\chi C}{1 + \nu C} \right] \quad (18)$$

where C is the nominal concentration of solvent water molecules, and χ the Flory-interaction parameter, which measures the strength of pairwise interactions between species.

The parameter χ is fitted to experimental data in the following form (Huggins, 1964):

$$\chi(T, \phi) = \chi_0 + \chi_1 \phi \quad (19)$$

where $\chi_0 = A_0 + B_0T$, $\chi_1 = A_1 + B_1T$ and $\phi = 1/(1 + \nu C)$. The symbol ϕ represents volume fraction of the polymer in the hydrogel. The values A_0 , A_1 , B_0 and B_1 vary for different monomers.

For a temperature-sensitive gel, the exact form of Π can be obtained by substituting Eq. (18) into Eq. (16) to give

$$\Pi = \frac{kT}{\nu} \left[\frac{\mu}{kT} - \ln \left(\frac{\nu C}{1 + \nu C} \right) - \frac{1}{1 + \nu C} - \frac{\chi_0}{(1 + \nu C)^2} - \frac{(1 - \nu C)\chi_1}{(1 + \nu C)^3} \right] \quad (20)$$

Using Eq. (14) to eliminate C , Eq. (20) is converted to

$$\Pi = \frac{kT}{\nu} \left[\frac{\mu}{kT} - \ln \left(\frac{J-1}{J} \right) - \frac{1}{J} - \frac{\chi_0 - \chi_1}{J^2} - \frac{2\chi_1}{J^3} \right] \quad (21)$$

where $J = \det(\mathbf{F})$ is the swelling ratio of the gel.

Eq. (20) and Eq. (21) relate the osmotic pressure with the solvent molecules concentration and deformation gradient respectively. The nominal stress is obtained by substituting Eq. (15) into Eq. (11)

$$S_{ik} = \frac{\partial W_{\text{stretch}}}{\partial F_{ik}} - \Pi J H_{ik} = NkT (F_{ik} - H_{ik}) - \Pi J H_{ik} \quad (22)$$

Note that we have used the mathematical relation $\frac{\partial J}{\partial F_{ik}} = J H_{ik}$ in order to derive Eq. (22), where \mathbf{H} is the transpose of \mathbf{F}^{-1} .

The true stress can be obtained through the relation

$$J \sigma_{ij} = S_{ik} F_{jk} \quad (23)$$

By substituting Eq. (22) into Eq. (23), we obtain

$$\sigma_{ij} = \frac{NkT}{J} (F_{ik}F_{jk} - \delta_{ij}) - \Pi \delta_{ij} \quad (24)$$

Further substitution of Eq. (21) into Eq. (24) yields an explicit form of the true stress

$$\sigma_{ij} = \frac{NkT}{J} (F_{ik}F_{jk} - \delta_{ij}) + \frac{kT}{\nu} \left[\ln \left(\frac{J-1}{J} \right) + \frac{1}{J} + \frac{\chi_0 - \chi_1}{J^2} + \frac{2\chi_1}{J^3} \right] \delta_{ij} - \frac{\mu}{\nu} \delta_{ij} \quad (25)$$

Eq. (25) relates the true stress to the deformation gradient. Rewriting Eq. (25), a general expression for the chemical potential for water molecules within the gel is obtained as

$$\mu = \frac{NkT\nu}{3J} (I-3) + kT \left[\ln \left(\frac{J-1}{J} \right) + \frac{1}{J} + \frac{\chi_0 - \chi_1}{J^2} + \frac{2\chi_1}{J^3} \right] - \frac{(\sigma_{11} + \sigma_{22} + \sigma_{33})\nu}{3} \quad (26)$$

where $I = F_{ik}F_{ik}$.

Using the equilibrium conditions given by Eq. (9), the analytical solution for a temperature-sensitive gel in a solution of chemical potential $\tilde{\mu}$ is

$$\mu = \tilde{\mu} \quad (27)$$

where the expression for μ is given by Eq. (26)

4. Finite element formulation

4.1. Static analysis

It can be seen from Eq. (17) that when $J=1$, the free energy density is singular. This singularity can be addressed by selecting any reference state with $J > 1$ (Hong et al., 2009). In our previous study on temperature-sensitive hydrogel (Ding et al., 2013), an isotropic swelling state was chosen as the initial state. As a result, it could not be used to study the deformation with an anisotropic initial state. In the present study, we choose an initial state with a deformation gradient in the form of:

$$\mathbf{F}_0 = \begin{bmatrix} \lambda_{0,1} & 0 & 0 \\ 0 & \lambda_{0,2} & 0 \\ 0 & 0 & \lambda_{0,3} \end{bmatrix} \quad (28)$$

By letting \mathbf{F}' be the deformation gradient relative to the chosen reference state, the deformation gradient \mathbf{F} is then expressed as follows:

$$\mathbf{F} = \mathbf{F}'\mathbf{F}_0 \quad (29)$$

In the present study, we will use subroutines in the commercial software ABAQUS to implement the above derived formulation. There are two options offered by ABAQUS to specify the nonlinear constitutive behavior of a hydrogel as user-defined materials, i.e. subroutines UHYPER and UMAT. The former (UHYPER) has been successfully implemented (Ding et al., 2013). However, UHYPER implementation is restricted to isotropic initial conditions. To circumvent this limitation, we implement our current finite element model using UMAT, which requires definition

of the true stress (Eq. 25) and tangent modulus tensor C_{ijkl} . The tangent modulus can be defined through the variation in the Kirchhoff stress

$$\delta(J\sigma_{ij}) = JC_{ijkl}\delta D_{kl} + J(\sigma_{kj}\delta W_{ik} - \sigma_{ik}\delta W_{kj}) \quad (30)$$

where the tensors $\delta\mathbf{D}$ and $\delta\mathbf{W}$ are the virtual rate of deformation and virtual spin tensor respectively, defined as:

$$\delta\mathbf{D} = \text{Sym}(\delta\mathbf{F} \cdot \mathbf{F}^{-1}) \quad (31)$$

$$\delta\mathbf{W} = \text{Skew}(\delta\mathbf{F} \cdot \mathbf{F}^{-1}) \quad (32)$$

By using Eq. (25), the variation of the Kirchhoff stress is calculated as follows

$$\begin{aligned} \delta(J\sigma_{ij}) = NkT \left\{ \frac{2}{3}J^{-\frac{1}{3}}\delta J + J^{\frac{2}{3}}\delta\tilde{B}_{ij} + \frac{\delta_{ij}}{N\nu} \left[-\frac{\mu}{kT} + \frac{1}{J-1} \right. \right. \\ \left. \left. + \ln\left(\frac{J-1}{J}\right) - \frac{4(A_1+B_1T)}{J^3} \right] \right. \\ \left. + \frac{(A_0-A_1) + (B_0-B_1)T}{J^2} \right\} \delta J \end{aligned} \quad (33)$$

It can be shown mathematically that

$$\delta J = J\delta D_{kk} \quad (34)$$

$$\delta\tilde{B}_{ij} = T_{ijkl} \left(\delta D_{kl} - \frac{\delta_{kl}}{3}\delta D_{kk} \right) + \tilde{B}_{kj}\delta W_{ik} - \tilde{B}_{ik}\delta W_{kj} \quad (35)$$

where the fourth order tensor \mathbf{T} is defined as

$$T_{ijkl} = \frac{1}{2}(\tilde{B}_{jl}\delta_{ik} + \tilde{B}_{ik}\delta_{jl} + \tilde{B}_{jk}\delta_{il} + \tilde{B}_{il}\delta_{jk}) \quad (36)$$

Substituting Eq. (34) and Eq. (35) into Eq. (33), an explicit expression for the tangent modulus tensor at the current state is obtained as

$$\begin{aligned} C_{ijkl} = NkT \left\{ J^{-\frac{1}{3}}T_{ijkl} + \frac{1}{N\nu} \left[-\frac{\mu}{kT} + \frac{1}{J-1} + \ln\left(\frac{J-1}{J}\right) \right. \right. \\ \left. \left. - \frac{4(A_1+B_1T)}{J^3} + \frac{(A_0-A_1) + (B_1-B_0)T}{J^2} \right] \delta_{ij}\delta_{kl} \right\} \end{aligned} \quad (37)$$

With Eq. (25) and Eq. (37), we define the material model using user-defined subroutine UMAT in ABAQUS.

The free energy density function introduces five material parameters A_0 , A_1 , B_0 , B_1 and $N\nu$. The values of A_0 , A_1 , B_0 and B_1 depend on the type of monomers, while $N\nu$ is a dimensionless measure of the polymer crosslink density in the dry network. The values of these parameters for poly(N-isopropyl acrylamide) (PNIPAM) are provided by Afroze et al. (2000) to be

$$\begin{aligned} A_0 = -12.947, A_1 = 17.92, B_0 = 0.04496/K, B_1 \\ = -0.0569/K \end{aligned} \quad (38)$$

where K is the unit of temperature in Kelvin.

We adopt the above properties of PNIPAM gels and set $N\nu = 0.01$ in the static numerical examples presented herein. To fully define the material in the subroutine, we also need to provide the initial temperature T_0 , the initial chemical potential of the external solution μ_0 , and the corresponding swelling ratios $\lambda_{0,1}$, $\lambda_{0,2}$, $\lambda_{0,3}$ in the x , y , z directions respectively. For an equilibrium state, these values need to satisfy Eq. (25).

4.2. Transient analysis

Recently, modeling the mass transport in gel as an equivalent heat transfer process has attracted much attention for its simplicity and wide applicability. However this method cannot be directly applied to temperature-sensitive gels as the kinetics of a temperature sensitive hydrogel is driven by two separate processes: heat transfer and mass diffusion. A different method is to define user elements (Chester et al., 2015). Alternatively, noting that the heat transfer process is usually much faster than the mass diffusion process (Chester, 2011), it is an appropriate approximation to regard the heat transfer process as an instantaneous process. After which, the swelling kinetics of the gel structure may be regarded as the migration of solvent molecules within and across the material boundary isothermally. An illustration of this approximation is given in Fig. 2. The dynamic deformation process (1) is generally referring to the process from state A to state C, during which both the temperature and chemical potential of the solution changes. Owing to the assumption that heat transfer is a much faster process, we decompose the above process into two consecutive steps: the first being heat transfer, represented by process (2) and second being mass diffusion, represented by process (3). A virtual intermediate state B is defined as the state at which process (2) has finished while process (3) has not started. In this state, the temperature in the gel is homogenous and equal to the temperature of the surroundings, whereas the chemical potential is also homogenous but different from the surrounding solutions. The exact value of the chemical potential may be calculated by Eq. (26). As mentioned earlier, since process (2) is much faster, and the gel material does not undergo much deformation, we will only model process (3) as an approximation to process (1).

During the mass diffusion process, the flux relates to the gradient of chemical potential by the following equation (Hong et al., 2008)

$$j_i = -\frac{cD}{kT} \frac{\partial \mu}{\partial x_i} = -cD \frac{\partial \bar{\mu}}{\partial x_i} \quad (39)$$

where $c = C/J$ is the current solvent concentration, D the diffusion coefficient, and $\bar{\mu} = \mu/kT$ the dimensionless chemical potential.

The conservation of the mass may be written as

$$\int_V \frac{1}{J} \frac{dC}{dt} dV + \int_S j_k n_k dS = 0 \quad (40)$$

By using the incompressibility condition given by Eq. (14), we rewrite Eq. (40) as

$$\int_V \frac{1}{J} \frac{dJ}{dt} dV + \int_S v j_k n_k dS = 0 \quad (41)$$

An expression for $\frac{\partial J}{\partial t}$ is required to implement Eq. (41). To obtain such an expression, we rewrite Eq. (26) in dimensionless form as

$$\bar{\mu} = \frac{N\nu}{3J} (\bar{J}^{\frac{2}{3}} - 3) + \left[\ln\left(\frac{J-1}{J}\right) + \frac{1}{J} + \frac{\chi_0 - \chi_1}{J^2} + \frac{2\chi_1}{J^3} \right] - \bar{\sigma} \quad (42)$$

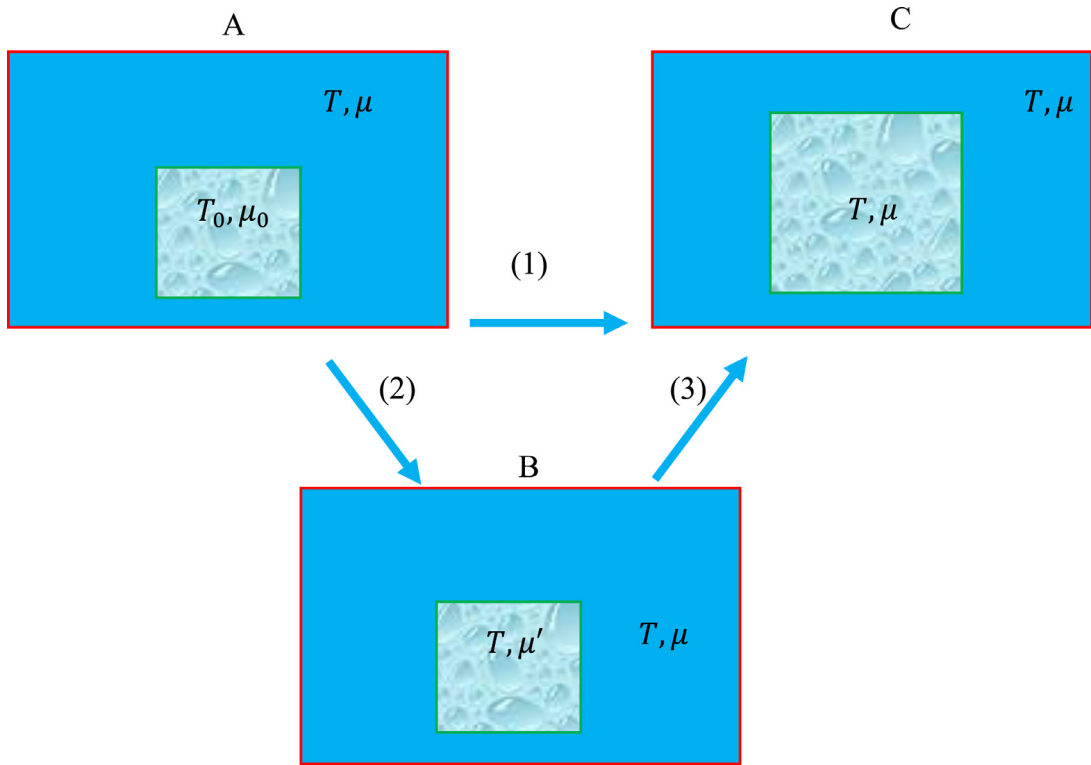


Fig. 2. An illustration to approximate the swelling process as a mass diffusion process. Generally, heat transfer is a much faster process compared to mass diffusion. Thus we approximate the dynamic swelling process (1) as a heat transfer process (2) followed by a mass diffusion process (3). And since process (2) is much faster and the gel material did not undergo much deformation during process (2), we only model process (3) as an approximation to process (1).

where $\bar{\mu} = \mu/kT$, $\bar{I} = IJ^{-2/3}$ is the deviatoric invariant, $\bar{\sigma} = \bar{\sigma}_{11} + \bar{\sigma}_{22} + \bar{\sigma}_{33}/3$ is the dimensionless mean stress, and $\bar{\sigma}_{ii} = \sigma_{ii}/(kT/v)$.

Using chain rule, and assuming $J = f(\bar{I}, \bar{\sigma}, \bar{\mu})$ in Eq. (42), we write $\frac{dJ}{dt}$ as

$$\frac{dJ}{dt} = \frac{\partial J}{\partial \bar{\mu}} \frac{d\bar{\mu}}{dt} + \frac{\partial J}{\partial \bar{I}} \frac{d\bar{I}}{dt} + \frac{\partial J}{\partial \bar{\sigma}} \frac{d\bar{\sigma}}{dt} \quad (43)$$

Combining Eqs. (41) and (43), the governing equation becomes

$$\int_V \frac{1}{J} \frac{\partial J}{\partial \bar{\mu}} \frac{d\bar{\mu}}{dt} dV + \int_S v_j j_k n_k dS = - \int_V \frac{1}{J} \left(\frac{\partial J}{\partial \bar{I}} \frac{d\bar{I}}{dt} + \frac{\partial J}{\partial \bar{\sigma}} \frac{d\bar{\sigma}}{dt} \right) dV \quad (44)$$

The governing equations for the heat transfer process in a solid are given as follows

$$q_i = -k \frac{\partial T}{\partial x_i} \quad (45)$$

where $c_p = dU/dt$ is the specific heat capacity.

Comparing Eq. (39) and Eq. (44) with Eq. (45) and Eq. (46), we can see that the mass transport process may be studied as a heat transfer process by the following equivalence

$$\rho = \frac{1}{J} \quad (47)$$

$$c_p = \frac{\partial J}{\partial \bar{\mu}} \quad (48)$$

$$T = \bar{\mu} \quad (49)$$

$$k = \frac{(J-1)}{J} D \quad (50)$$

$$r = -\frac{1}{J} \left(\frac{\partial J}{\partial \bar{I}} \frac{d\bar{I}}{dt} + \frac{\partial J}{\partial \bar{\sigma}} \frac{d\bar{\sigma}}{dt} \right) \quad (51)$$

Using Eq. (42), we obtain the explicit expression for the partial derivative terms as

$$\frac{\partial J}{\partial \bar{\mu}} = \frac{\partial J}{\partial \bar{\sigma}} = \frac{9J^4(J-1)}{Nv\bar{I}(1-J)J^{3/3} + 9Nvj^3 + 9[(1-Nv) + 2(\chi_1 - \chi_0)]J^2 + 18(\chi_0 - 4\chi_1)J + 54\chi_1} \quad (52)$$

$$\int_V \rho c_p \frac{dT}{dt} dV + \int_S q_k n_k dS = \int_V r dV \quad (46)$$

$$\frac{\partial J}{\partial \bar{I}} = -\frac{Nv}{3J^{1/3}} \frac{\partial J}{\partial \bar{\sigma}} \quad (53)$$

Every term is now expressed in terms of the quantities that are accessible as field variables in ABAQUS. To implement the present methodology in ABAQUS, we have adopted UHYPER for temperature-sensitive gel to govern the mechanical behavior. The choice of UHYPER over UMAT is due to simplicity of implementation of UHYPER in the diffusion-heat transfer model as the main purpose is to show the validity of the assumption in our analysis. Alternatively, the interested reader may implement the mechanical properties using UMAT.

The equivalent heat transfer properties, i.e. heat capacity, conduction coefficient and density are defined as functions of stretch invariants using subroutine USDFLD. The heat source term given by Eq. (51) is defined through subroutine HETVAL. With the concurrent application of these three subroutines, the kinetics of gel deformation can now be studied using ABAQUS using a fully coupled temperature-displacement analysis.

5. Numerical examples for static analysis

To verify the correctness of the developed finite element subroutine formulation and highlight the advantage of UMAT over UHYPER, several numerical examples are provided in this section.

5.1. Free swelling

The analytical solution may be obtained by searching the value of J at which the free energy functions are minimized at a certain temperature T . It can also be derived analytically. In the free swelling process, the chemical potential for water molecules given by Eq. (26) may be simplified as

$$\mu = \frac{NkTv}{J} (J^{\frac{2}{3}} - 1) + kT \left[\ln \left(\frac{J-1}{J} \right) + \frac{1}{J} + \frac{\chi_0 - \chi_1}{J^2} + \frac{2\chi_1}{J^3} \right] \quad (54)$$

Using the equilibrium conditions given in Eq. (27) and with the fact that the chemical potential of water is $\tilde{\mu} = 0$, the analytical solution may be written as:

$$\frac{NkTv}{3J} (J^{\frac{2}{3}} - 3) + kT \left[\ln \left(\frac{J-1}{J} \right) + \frac{1}{J} + \frac{\chi_0 - \chi_1}{J^2} + \frac{2\chi_1}{J^3} \right] = 0 \quad (55)$$

The numerical solutions obtained using UHYPER and UMAT are plotted in Fig. 3. In this problem we have chosen a value of $Nv = 0.01$. For verification purpose, the experimental data reported by (Oh et al., 1998) is also plotted. As shown in Fig. 3 the numerical results using UMAT are in good agreement with the analytical solutions, the numerical results using UHYPER and the experimental data. It should be noted that for a discontinuous phase transition, FEM is unable to overcome the turning points. To obtain both parts of the phase transition curve, we employ the method proposed by Ding et al. (2013) to start simulation from both ends, which terminate at points A and B.

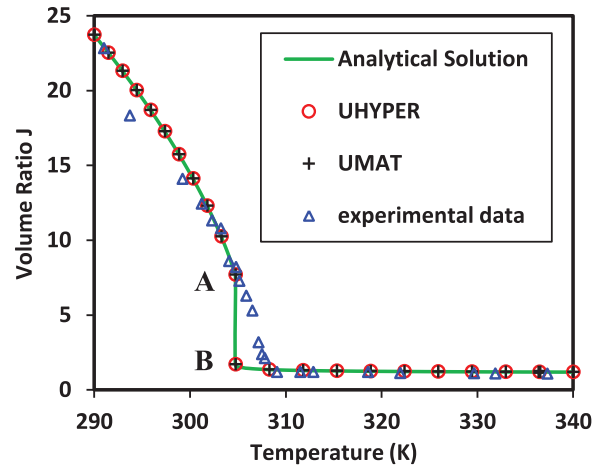


Fig. 3. Volume of free-swelling hydrogel as a function of temperature. The solid curve is obtained analytically for the free swelling case. The circles and asterisks are corresponding numerical prediction using UHYPER and UMAT, respectively. The triangles represent experimental results from Oh et al. (1998).

5.2. Uniaxial constraint

Deformation under a uniaxial constraint refers to the swelling gel being fixed vertically and free to swell in the other two directions. In this case, the lateral stretches are the same, while the longitudinal stretch in the third direction is constant, i.e. $\lambda_1 = \lambda_2 = \lambda$, $\lambda_3 = \lambda_0$. Thus $J = \lambda^2 \lambda_0$ and $I = 2\lambda^2 + \lambda_0^2 = \frac{2J}{\lambda_0} + \lambda_0^2$.

To illustrate the constraints of UHYPER, we consider two cases, i.e. $\lambda_0 = 1$ and $\lambda_0 = 2$. Uniaxial constrained swelling induces stress in the longitudinal direction, while lateral stresses are zero. Using Eq. (25), and the condition $\sigma_{11} = \sigma_{22} = 0$, the parameter to define the initial state needs to satisfy the following equation.

$$\frac{NkT_0}{\lambda_1^2 \lambda_0} (\lambda_1^2 - 1) + \frac{kT_0}{v} \left[\ln \left(\frac{\lambda_1^2 \lambda_0 - 1}{\lambda_1^2 \lambda_0} \right) + \frac{1}{\lambda_1^2 \lambda_0} + \frac{\chi_0 - \chi_1}{(\lambda_1^2 \lambda_0)^2} + \frac{2\chi_1}{(\lambda_1^2 \lambda_0)^3} \right] - \frac{\tilde{\mu}}{v} = 0 \quad (56)$$

The analytical solution may also be derived based on the chemical potential of water $\tilde{\mu} = 0$,

$$\frac{Nv}{\lambda_1^2 \lambda_0} (\lambda_1^2 - 1) + \left[\ln \left(\frac{\lambda_1^2 \lambda_0 - 1}{\lambda_1^2 \lambda_0} \right) + \frac{1}{\lambda_1^2 \lambda_0} + \frac{\chi_0 - \chi_1}{(\lambda_1^2 \lambda_0)^2} + \frac{2\chi_1}{(\lambda_1^2 \lambda_0)^3} \right] = 0 \quad (57)$$

Alternatively, the analytical solution can also be obtained by searching the value of J at which the global minimum of the free energy functions is achieved at a certain temperature T . The numerical calculations obtained using UHYPER and UMAT are also plotted in Fig. 4 together with the analytical solution. As seen from Fig. 4, UHYPER is only applicable to the process below the phase transition temperature in the case $\lambda_0 = 2$, and not applicable for the case

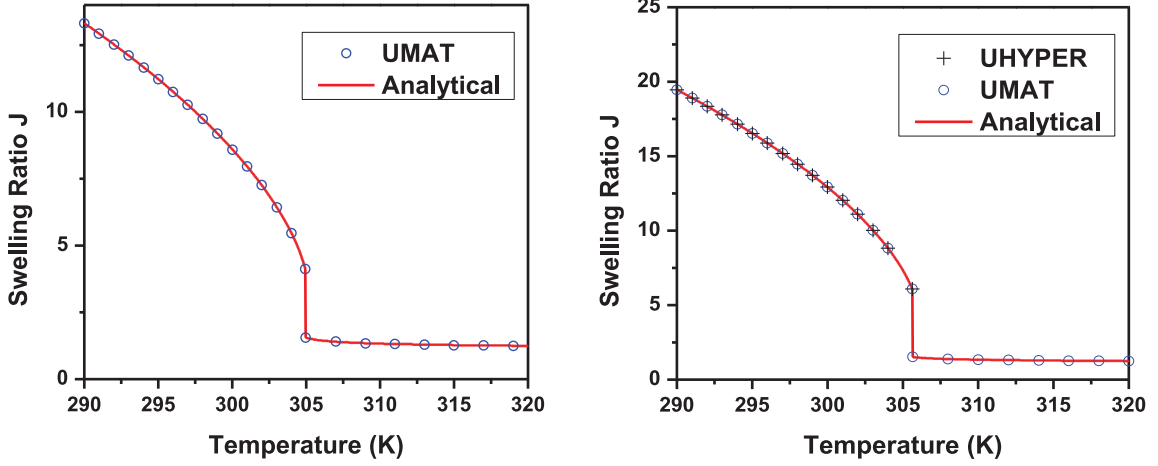


Fig. 4. Volume of the uniaxial constrained swelling hydrogel as a function of temperature. (a) Fixed stretch in longitudinal direction $\lambda_0 = 1$; (b) Fixed stretch in longitudinal direction $\lambda_0 = 2$. The other two directions are free to swell. UHYPER is only applicable to the process below the phase transition temperature in the case $\lambda_0 = 2$, and entirely not applicable for the case $\lambda_0 = 1$.

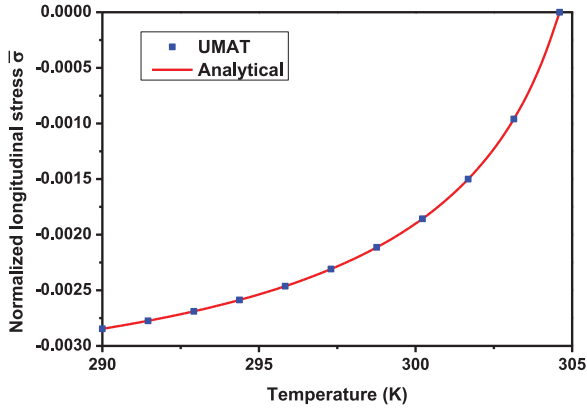


Fig. 5. Normalized longitudinal stress during uniaxial swelling process.

$\lambda_0 = 1$. As mentioned earlier, this is due to the fact that the reference state for UHYPER has to be isotropic swelling. When $\lambda_0 = 1$ is fixed, the corresponding isotropic swelling state is the dry state and $J = 1$. This would encounter singularity in the calculation of free energy density. When $\lambda_0 = 2$, there is no isotropic state at a temperature higher than the phase transition temperature. Thus UHYPER is not applicable.

It is obvious that the only non-zero true stress during the uniaxial deformation process is the normal stress in the third direction σ_{33} . In the uniaxial deformation process, Eq. (24) may be written as:

$$\sigma_{11} = \sigma_{22} = \frac{NkT}{\lambda_0 \lambda_1^2} (\lambda_1^2 - 1) - \Pi \quad (58)$$

$$\sigma_{33} = \frac{NkT}{\lambda_0 \lambda_1^2} (\lambda_0^2 - 1) - \Pi \quad (59)$$

Using the condition $\sigma_{11} = \sigma_{22} = 0$ to eliminate Π , we obtain

$$\sigma_{33} = \frac{NkT}{\lambda_0 \lambda_1^2} (\lambda_0^2 - \lambda_1^2) \quad (60)$$

Table 1
Physical properties of gel material.

	Density (kg/m ³)	Heat capacity (J/kgK)	Thermal conductivity (W/mK)
Network	1.2×10^3	2×10^4	2
Solvent	1×10^3	4.2×10^3	$-1.05 \times 10^{-5} T^2 + 7.98 \times 10^{-3} T - 8.38 \times 10^{-1}$

Table 2
Physical parameters for gel with different compositions. NIPA and SA stands for N-isopropylacrylamide and sodium acrylate, respectively.

No.	NIPA:SA	Nv	D (m ² /s)
B07	90:10	0.003	7×10^{-8}
B03	98:2	0.01	1.2×10^{-8}

which gives the true stress as a function of temperature T and stretch λ_1 . Eq. (60) can be used to verify the correctness of the stress obtained using the presently proposed methodology. By using either the analytical solution given by Eq. (57) or directly using the numerical obtained from the output of ABAQUS, we can obtain the value for λ_1 at any temperature T , and substitute these values into Eq. (60) to evaluate the stress. We can also read the stress at any temperature from the numerical simulation results. The stress during the uniaxial swelling process calculated using Eq. (60) and obtained via our subroutine has been plotted in Fig. 5. As can be clearly observed, they are in good agreement. For convenience we have normalized the stress by kT_0/ν , with $T_0 = 300$ K.

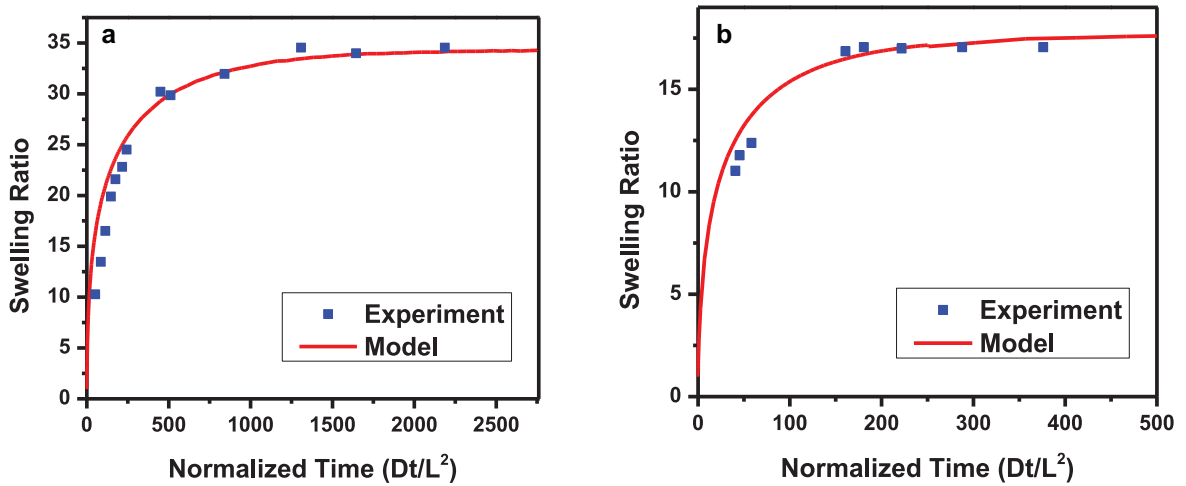


Fig. 6. Comparison of simulation results with experimental results. Solid line represents simulation results, while discrete points represent experimental data (Zhuang et al., 2000). (a) Swelling ratio as a function of time for sample NO. B07 in (Zhuang et al., 2000), $Nv = 0.003$ $D = 7E-8$ m^2/s (b) Swelling ratio as a function of time for sample NO. B03 in (Zhuang et al., 2000), $Nv = 0.01$ $D = 1.2E-8$ m^2/s . The simulation model is a cylinder with a diameter of 1 cm and thickness 2 mm, and dry gels are immersed in water at 297 K.

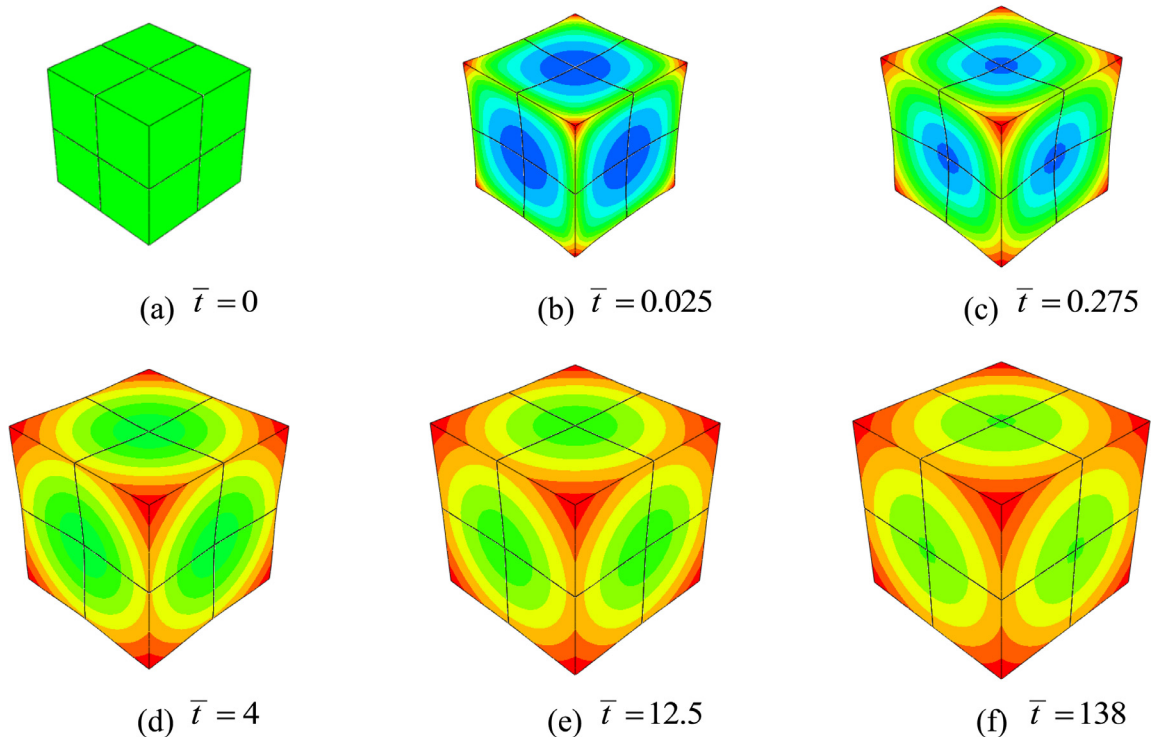


Fig. 7. Displacement contour plots for non-dimensional free swelling cubic gel based on method 1 at various time intervals. The plots are of similar scale to show the large deformation process. In this method, heat transfer is treated as an instantaneous process.

6. Verifications of the transient model

6.1. Comparison with experimental results

To verify the correctness of the transient model, we compare simulation results with available experimental measurements reported by (Zhuang et al., 2000). In the

experiments, the gel was cut into disks with thickness of 2 mm and diameter of 1 cm. The results were reported using mass swelling ratio. Using the physical parameters reported in the literature (Bae et al., 1989; Bird et al., 2007; Prokop et al., 2003; Salmerón Sánchez et al., 2004; Wagner and Pruß, 2002), we convert the mass swelling ratio to volume swelling ratio. The physical properties for the

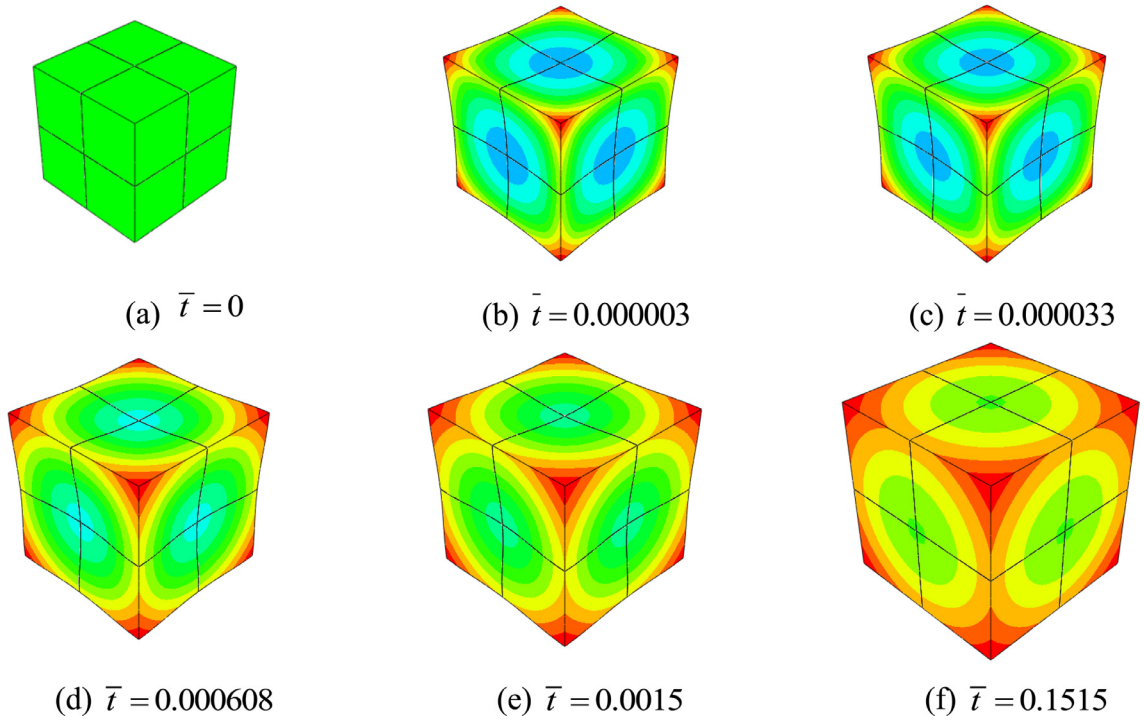


Fig. 8. Displacement contour plots for non-dimensioned free swelling cubic gel based on method 2 at various time intervals. The plots are of similar scale to show the large deformation process. In this method, mass diffusion is treated as an instantaneous process.

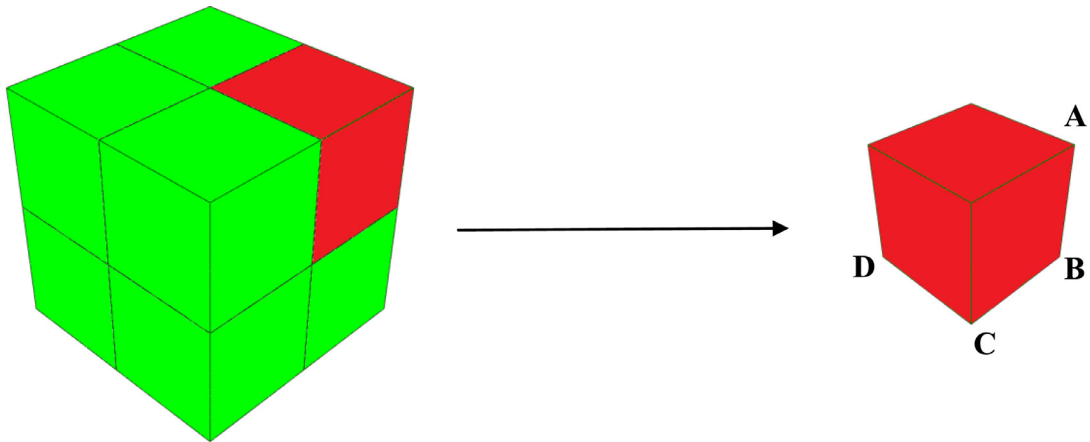


Fig. 9. Schematic illustrations of the four chosen points.

polymer and solvent phases are summarized in Table 1. Since the values for Nv and D are not given explicitly in the references, we perform fitting to obtain these values. Table 2 summarizes the parameter values for gels with different compositions. We have chosen the isotropic state with initial stretch 1.0001 as the dry state to avoid singularity of the free energy function when $J=1$. It is observed from Table 2 that different Sodium Acrylate contents can result in different polymer chains density (Nv) and diffusion coefficient (D). The experimental measured and simulated results for the variation of swelling ratio with re-

spect to time are shown in Fig. 6. Good agreement between experimental results and simulation results for both samples with different Sodium Acrylate contents has been observed.

6.2. Verification of assumption of process rates

In Section 4.2, we have assumed that heat transfer is a much faster process than mass diffusion. We will now verify this assumption. The total time for heat transfer can be obtained by treating mass diffusion as an instantaneous

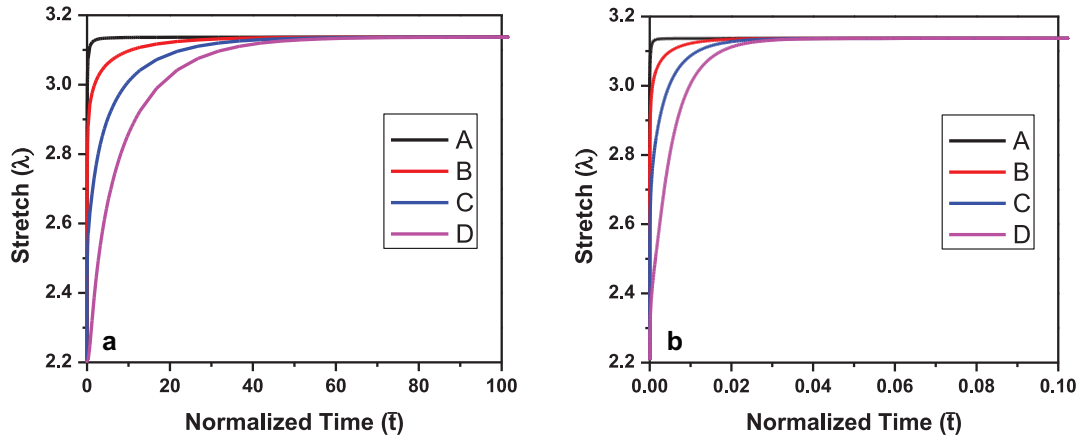


Fig. 10. Stretches at the four chosen points as a function of time. (a) Method 1: treating heat transfer as an instantaneous process (b) Method 2: treating diffusion as an instantaneous process.

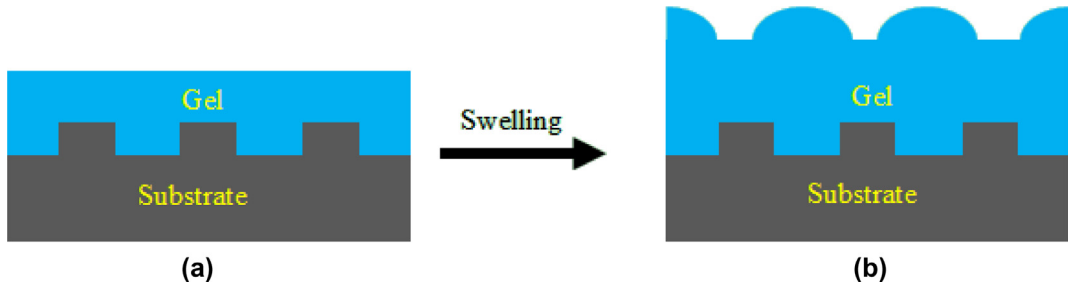


Fig. 11. Schematic illustration of substrate directed creasing. (a) Gel is fixed on substrate with step edge; (b) After swelling, the position of the crease is directed by the step edge position of the substrate.

process. We first assume that the transfer of heat energy is due to conduction of heat in both the polymer network as well as solvent molecules. Next we assume deformation to be temperature driven as the gel is pre-swollen to a state of homogenous chemical potential. The heat conduction equation is given by Eqs. (45) and (46).

The thermal properties are taken to be a mixture of both components. The thermal conductivities of the polymer network and solvent are assumed to be isotropic, with conductivity of solvent taken to be dependent on temperature as shown in Table 1. The conductivity, density and heat capacity are expressed as

$$k^m = \phi k^p + (1 - \phi)k^s \quad (61)$$

$$\rho^m = \phi \rho^p + (1 - \phi)\rho^s \quad (62)$$

$$c_p^m = \phi c_p^p + (1 - \phi)c_p^s \quad (63)$$

where k , ρ and c_p are the conduction coefficient, density and specific heat capacity respectively. The superscripts m , p and s represent the mixture, polymer network and solvent respectively. Their values are given in Table 1

Now we simulate the deformation process as a heat transfer process with the concurrent use of UHYPER and USDFLD, based on the two methods described above. Consider the process when a cubic gel of unit length is immersed in water and undergoes a temperature drop from

303 K to 283 K. Using the method proposed in Section 4.2, this process is equivalent to a process where the normalized chemical potential increases from -0.017 to 0 at 283 K. Based on Eq. (54), we can calculate that the cubic gel will swell from the initial stretch of 2.200 to 3.137.

In the simulation where mass diffusion is assumed dominant (method 1, which assumes heat transfer is instantaneous), we define a dimensionless time $\bar{t} = Dt/L^2$, where D is the diffusion coefficient given in Table 2 and L is the length of the cube. In the simulation where heat transfer is assumed dominant (method 2, which assumes diffusion is instantaneous), we employ the same characteristic time for non-dimensionalization. This translates to $\bar{t} = 0.144 \times De t/L^2 = Dt/L^2$, where $De = k^p/(\rho^p c_p^p)$. This equality can be easily verified with the physical properties provided in Table 1 and Table 2.

Static analysis assumes that the gel will remain homogenous during the swelling process, which is not the case. To see exactly how the gel is deforming, several representative states have been selected and shown in Figs. 7 and 8. It is observed that the corner regions of the cubic gel will deform first because of comparatively larger contact surface with the solution. In addition, the difference in swelling time between both sets of results highlight the differences in swelling rates between heat transfer and mass diffusion.

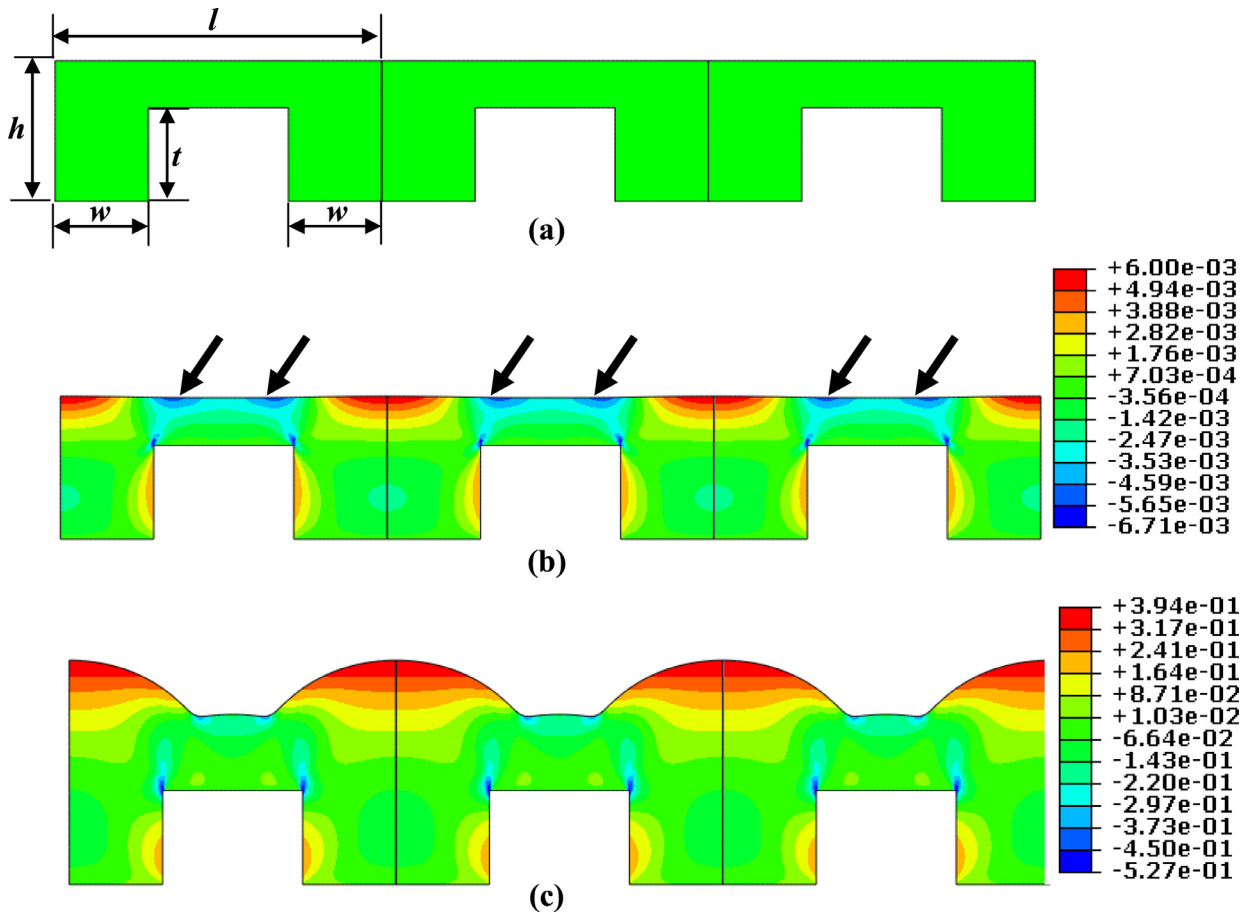


Fig. 12. In-plane strain distribution at (a) initial state (b) just before creasing (c) swollen state. The unit cell has dimensions $l:h:w:t = 7:4:3:2$, and gel undergoes a temperature drop from 303 K to 283 K.

To have a better idea of how different parts of the gel deform at varying rates, four points have been chosen for further study. Consider one quarter of the cubic as highlighted in red, the points A, B, C, and D are chosen as shown in Fig. 9.

The change of stretches at points A, B, C and D with respect to time are plotted in Fig. 10(a) and (b) for Method 1 and Method 2.

For both methods, it is evident that while the initial rates of swelling are different, the eventual uniform distribution of chemical potential and temperature would lead to homogenous swelling at all points. Therefore the steady-state equilibrium stretch is consistent with the analytical solution calculated from Eq. (55), thus verifying that the final state of the transient analysis approaches the theoretical equilibrium state.

The total swelling time is the time taken for the center of the cube (Point D) to reach equilibrium. Comparing the total swelling time using method 1 and method 2, we can observe that the time taken for diffusion is about three orders of magnitude slower than that for heat transfer. This verifies our earlier assumption that the mass diffusion process is much slower as compared to the heat transfer pro-

cess. Thus it is an appropriate assumption to treat the heat transfer process as an instantaneous one, in the event that both processes are present during the deformation.

7. Applications

7.1. Substrate directed creasing pattern

The swelling induced surface instability of hydrogels has been studied experimentally and theoretically. The buckling pattern depends on the mechanical and geometrical properties of the swelling material (Liu et al., 2011). However, it has been reported that the creasing pattern of surface-attached hydrogel can be directed by the underlying rigid substrates (Kim et al., 2010), as shown in Fig. 11.

As discussed by (Toh et al., 2015), dynamic finite element simulations have the tendency to terminate abruptly due to surface wrinkling in transient analysis. Thus we only perform static analysis using UMAT with plain strain elements. The in-plane strain distribution patterns just before the onset of wrinkling and at the final state are shown in Fig. 12. As shown in the figure, compressive in-plane strain in the region (black arrow in Fig. 12(b)) during swelling

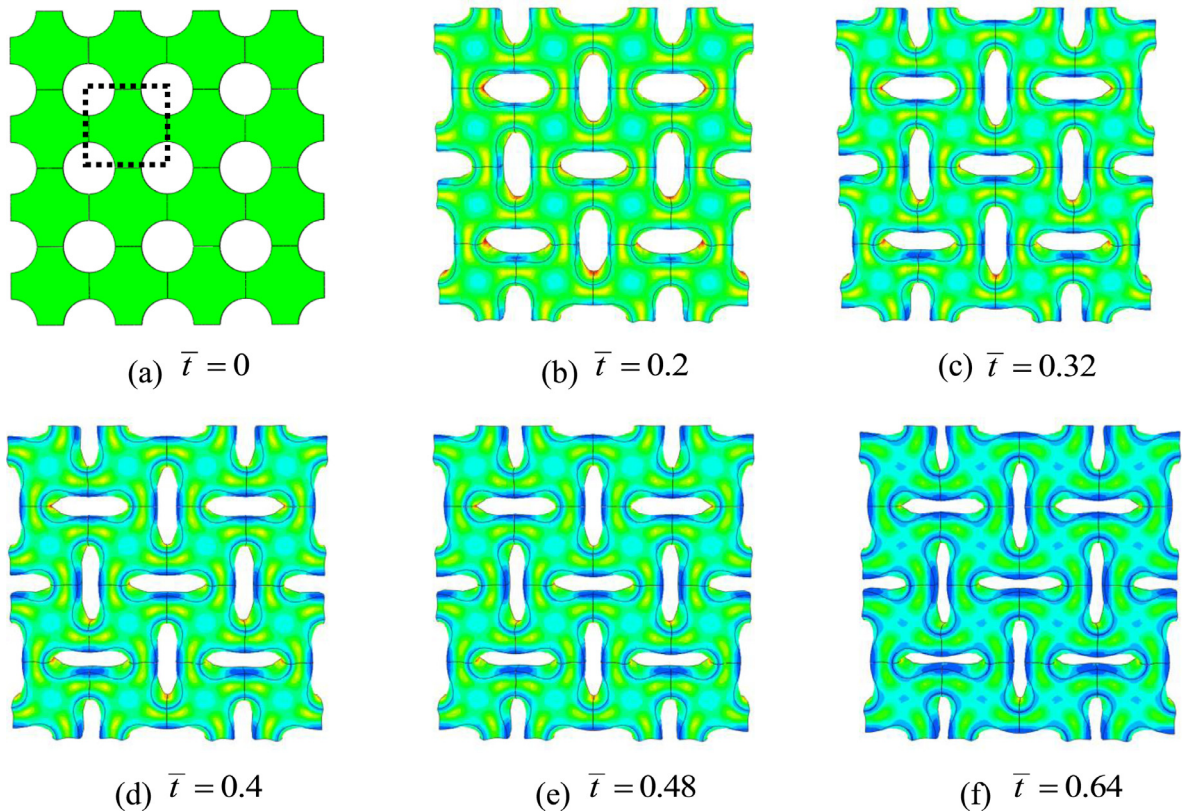


Fig. 13. The von-Mises stress distribution during the bifurcation process. The side of the unit cell is 3, the radius of the hole is 1, and the thickness of the film is 1. Symmetric boundaries are applied at the side accordingly while the bottom surface is fixed. The gel undergoes temperature drop from 303 K to 283 K.

induces the formation of a crease some distance away from the step edge. This indicates that the wrinkling patterns can be guided (or influenced) by the topographic feature of the substrate.

7.2. Bifurcation

When a thin film containing holes in a square array is exposed to a solvent as shown in Fig. 13, a diamond plate pattern is observed. Circular holes are deformed into elliptical slits and neighboring slits are mutually perpendicular (Zhang et al., 2008). Owing to several attractive mechanical and acoustic applications, many researchers have tried to explain the gel behavior using the thermodynamic model (Ding et al., 2013; Hong et al., 2009; Okumura et al., 2014). However, these studies are all equilibrium steady-state analyses. Here we consider a unit cell containing quadrants of four neighboring holes as shown in Fig. 13(a), where the initial temperature is fixed at 303 K. The side of the unit cell is 3, the radius of the hole is 1 and the thickness of the film is 1, as shown in Fig. 13(a). Note that the unit does not matter, since we are using non-dimensional quantities, and in this example the thickness is taken as the characteristic length when normalizing time. To enhance the visualization, we examine snapshots of the unit cell at several time intervals.

The deformation and stress distribution at various dimensionless times are shown in Fig. 13. It is observed that the von-Mises stress at the slit tip is much higher compared with other regions, which is similar to a crack tip. As Zhang et al. (2008) did not provide information on the deformation pattern transformation or the value of diffusion coefficient, we are unable to compare or verify our results with the experimental observation. However, our method can be used to control the fabrication process if it is subsequently verified to work well.

7.3. Buckling of swelling gel

The patterns arising from the differential swelling of the gels have been investigated experimentally and theoretically as a model for the differential growth of living tissues (Liu et al., 2010; Liu et al., 2013; Mora and Boudaoud, 2006). Here we consider the case study of a swelling annulus gel fixed at the inner wall. It has been generally accepted that the buckling pattern depends on the ratio between inner radius and outer radius of the annulus gel (Mora and Boudaoud, 2006). However, what static analyses have failed to show, is that from the onset of buckling to the time the gel reaches the equilibrium mode shape, the gel transits between different mode shapes. In

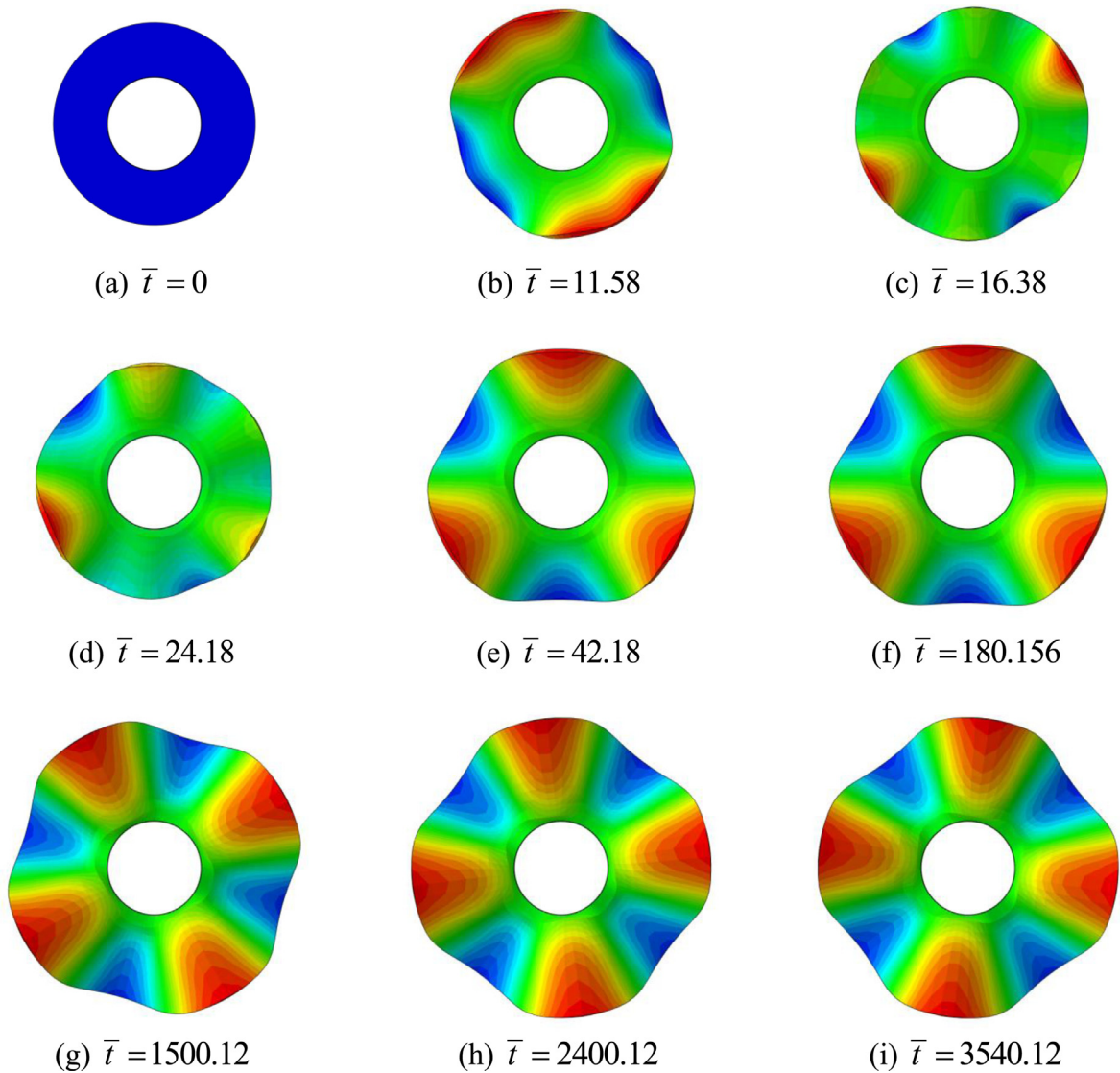


Fig. 14. The contour plot of y -displacement showing the evolution of wrinkles of an annulus with height 5 mm, inner radius 50 mm and outer radius 75 mm. The transition of mode shapes can be observed from (a) to (g) and the propagation of a travelling wave is seen in (g) to (i).

addition, when a gel first reaches the equilibrium mode shape, the buckling waves propagate through a twisting motion. Fig. 14 shows both interesting phenomena which are not observable in static analyses.

For a better understanding of the swelling process, we plot the stress and vertical displacement of selected points as shown in Fig. 15. It can be observed from Fig. 14 that mode transitions often occur within the first 50 units of time. Also, there is substantial fluctuation in the stress and displacement curves, see Fig. 15. Following this, the annulus will swell and take on the third mode for about 500 units of time. At about $\bar{t} = 700$, the annulus changes to the fourth mode and starts to rotate at about $\bar{t} = 1500$. This mode transition phenomenon has been observed in earlier simulations carried out for polymeric gels

(Toh et al., 2013). Though there are mode transitions, the equilibrium mode shape is consistent with the experimental observations (Mora and Boudaoud, 2006) and static simulations (Liu et al., 2013). To our best knowledge, there is no experimental report for the rotational instability of the swelling annulus, but such instability has been predicted numerically (Freund, 2000) and observed experimentally (Holmes et al., 2011) for a swelling disk. Due to the axial symmetry, there are numerous energy favorable orientations for the equilibrium mode shape. A random perturbation may lead to re-orientations into other minimum energy states. In our simulations, the dynamics of diffusion and swelling may result in perturbation significant enough to cause a travelling buckle wave to propagate around the annulus.

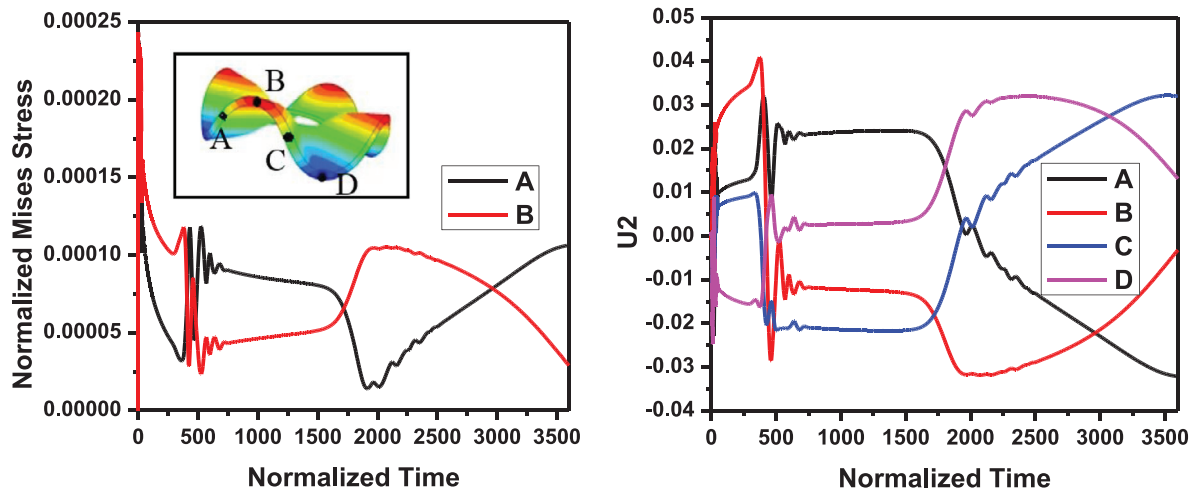


Fig. 15. The von-Mises stress (a), and vertical displacement (b), as a function of time for the selected points during the swelling process. Mode transitions often occur within the first 50 units of time. At around $\bar{t}=700$, the annulus takes on the fourth mode and starts to rotate at around $\bar{t}=1500$.

8. Concluding remarks

The prevalent approach of modeling hydrogels as hyperelastic materials reduces the amount of work required for finite element implementation. However, this convenience comes with a trade-off and requires the gel be isotropically stretched in the initial conditions. To overcome this constraint, we have developed a more robust model for simulating temperature sensitive hydrogels by defining its constitutive equations using UMAT, rather than a hyperelastic material using UHYPER. With this highly robust subroutine, it becomes possible to simulate cases which find UHYPER deficient. This approach is verified with analytical solutions for numerical accuracy, as well as with experimental results for theoretical validity.

In addition, we have proposed a model for the transient swelling simulation of temperature sensitive hydrogels, which is a coupled process involving heat transfer and diffusion of solvent molecules. By showing that the heat transfer process is three orders of magnitude faster than the mass diffusion process, we have validated and employed the assumption that heat transfer may be taken to be an instantaneous process.

Using the above two developments, we have provided several numerical examples to illustrate the potential applications of this work, including surface creasing, bifurcation and buckling of gels. These examples have provided deeper insights into interesting new physical phenomena observed in experiments. In the buckling of gels, transient analysis has shed light on two phenomena which static analysis is unable to show, namely the transition of mode shapes during the transient swelling process and the rotation of buckling waves upon reaching the equilibrium mode shape. These capabilities provide a valuable tool for further research into the development of novel and innovative applications of temperature sensitive hydrogels.

Acknowledgments

The authors would like to express their appreciation to the A*STAR Institute of High Performance Computing (IHPC) for providing all the necessary supercomputing resources. The authors are also grateful for the support from the National Natural Science Foundation of China through grant numbers 11372236, 11572236 and 11321062.

References

- Afroze, F., Nies, E., Berghmans, H., 2000. Phase transitions in the system poly(N-isopropylacrylamide)/water and swelling behaviour of the corresponding networks. *J. Mol. Struct.* 554, 14.
- Bae, Y.H., Okano, T., Kim, S.W., 1989. Insulin permeation through thermo-sensitive hydrogels. *J. Controlled Release* 9, 271–279.
- Bird, R.B., Stewart, W.E., Lightfoot, E.N., 2007. *Transport Phenomena*. John Wiley & Sons.
- Cai, S.Q., Suo, Z.G., 2011. Mechanics and chemical thermodynamics of phase transition in temperature-sensitive hydrogels. *J. Mech. Phys. Solids* 59, 20.
- Cai, S.Q., Suo, Z.G., 2012. Equations of state for ideal elastomeric gels. *EPL (Europhys. Lett.)* 97, 34009.
- Chester, S.A., 2011. *Mechanics of Amorphous Polymers And Polymer Gels*. Department of Mechanical Engineering, Massachusetts Institute of Technology, p. 356.
- Chester, S.A., Anand, L., 2010. A coupled theory of fluid permeation and large deformations for elastomeric materials. *J. Mech. Phys. Solids* 58, 1879–1906.
- Chester, S.A., Anand, L., 2011. A thermo-mechanically coupled theory for fluid permeation in elastomeric materials: Application to thermally responsive gels. *J. Mech. Phys. Solids* 59, 1978–2006.
- Chester, S.A., Di Leo, C.V., Anand, L., 2015. A finite element implementation of a coupled diffusion-deformation theory for elastomeric gels. *Int. J. Solids Struct.* 52, 1–18.
- De, S.K., Aluru, N.R., 2004. A chemo-electro-mechanical mathematical model for simulation of pH sensitive hydrogels. *Mech. Mater.* 36, 395–410.
- Ding, Z.W., Liu, Z.S., Hu, J.Y., Swaddiwudhipong, S., Yang, Z.Z., 2013. Inhomogeneous large deformation study of temperature-sensitive hydrogel. *Int. J. Solids Struct.* 50, 2610–2619.
- Drozdov, A.D., 2015. Volume phase transition in thermo-responsive hydrogels: constitutive modeling and structure–property relations. *Acta Mech.* 226, 1283–1303.
- Flory, P.J., 1953. *Principles of Polymer Chemistry*. Cornell University Press, Ithaca, NY.
- Freund, L., 2000. Substrate curvature due to thin film mismatch strain in the nonlinear deformation range. *J. Mech. Phys. Solids* 48, 1159–1174.

- Holmes, D.P., Roché, M., Sinha, T., Stone, H.A., 2011. Bending and twisting of soft materials by non-homogenous swelling. *Soft Matter* 7, 5188–5193.
- Hong, W., Liu, Z.S., Suo, Z.G., 2009. Inhomogeneous swelling of a gel in equilibrium with a solvent and mechanical load. *Int. J. Solids Struct.* 46, 3282–3289.
- Hong, W., Zhao, X.H., Suo, Z.G., 2010. Large deformation and electrochemistry of polyelectrolyte gels. *J. Mech. Phys. Solids* 58, 558–577.
- Hong, W., Zhao, X.H., Zhou, J.X., Suo, Z.G., 2008. A theory of coupled diffusion and large deformation in polymeric gels. *J. Mech. Phys. Solids* 56, 1779–1793.
- Huggins, M.L., 1964. Revised theory of high polymer solutions. *J. Am. Chem. Soc.* 86 3535–3440.
- Kang, M.K., Huang, R., 2010. A variational approach and finite element implementation for swelling of polymeric hydrogels under geometric constraints. *J. Appl. Mech.* 77, 061004.
- Kim, J., Yoon, J., Hayward, R.C., 2010. Dynamic display of biomolecular patterns through an elastic creasing instability of stimuli-responsive hydrogels. *Nat. Mater.* 9, 159–164.
- Lai, F., Li, H., 2011. Transient modeling of the reversible response of the hydrogel to the change in the ionic strength of solutions. *Mech. Mater.* 43, 287–298.
- Liu, Z., Hong, W., Suo, Z., Swaddiwudhipong, S., Zhang, Y., 2010. Modeling and simulation of buckling of polymeric membrane thin film gel. *Comput. Mater. Sci.* 49, S60–S64.
- Liu, Z.S., Swaddiwudhipong, S., Cui, F.S., Hong, W., Suo, Z.G., Zhang, Y.W., 2011. Analytical solutions of polymeric gel structures under buckling and wrinkle. *Int. J. Appl. Mech.* 03, 235–257.
- Liu, Z.S., Swaddiwudhipong, S., Hong, W., 2013. Pattern Formation in Plants via Instability Theory of Hydrogels *Soft Matter* 9, 11.
- Marcombe, R., Cai, S.Q., Hong, W., Zhao, X.H., Lapusta, Y.R., Suo, Z.G., 2010. A theory of constrained swelling of a pH-sensitive hydrogel. *Soft Matter* 6, 784–793.
- Mora, T., Boudaoud, A., 2006. Buckling of swelling gels. *Eur. Phys. J E* 20, 119–124.
- Oh, K.S., Oh, J.S., Choi, H.S., Bae, Y.C., 1998. Effect of cross-linking density on swelling behavior of NIPA gel particles. *Macromolecules* 31, 7328–7335.
- Okumura, D., Kuwayama, T., Ohno, N., 2014. Effect of geometrical imperfections on swelling-induced buckling patterns in gel films with a square lattice of holes. *Int. J. Solids Struct.* 51, 154–163.
- Prokop, A.F., Vaezy, S., Noble, M.L., Kaczowski, P.J., Martin, R.W., Crum, L.A., 2003. Polyacrylamide gel as an acoustic coupling medium for focused ultrasound therapy. *Ultrasound Med. Biol.* 29, 1351–1358.
- Salmerón Sánchez, M., Monleón Pradas, M., Gómez Ribelles, J.L., 2004. Thermal transitions in PHEA hydrogels by thermomechanical analysis. A comparison with DSC data. *Eur. Polym. J.* 40, 329–334.
- Toh, W., Ding, Z.W., Yong Ng, T., Liu, Z.S., 2015. Wrinkling of a polymeric gel during transient swelling. *J. Appl. Mech.* 82 061004–061004.
- Toh, W., Liu, Z.S., Ng, T.Y., Hong, W., 2013. Inhomogeneous large deformation kinetics of polymeric gels. *Int. J. Appl. Mech.* 05, 1350001.
- Toh, W., Ng, T.Y., Hu, J.Y., Liu, Z.S., 2014. Mechanics of inhomogeneous large deformation of photo-thermal sensitive hydrogels. *Int. J. Solids Struct.* 51, 4440–4451.
- Toh, W., Ng, T.Y., Liu, Z.S., Hu, J.Y., 2014. Deformation kinetics of pH-sensitive hydrogels. *Polym. Int.* 63, 1578–1583.
- Wagner, W., Pruß, A., 2002. The IAPWS formulation 1995 for the thermodynamic properties of ordinary water substance for general and scientific use. *J. Phys. Chem. Ref. Data* 31, 387–535.
- Zhang, Y., Matsumoto, E.A., Peter, A., Lin, P.C., Kamien, R.D., Yang, S., 2008. One-step nanoscale assembly of complex structures via harnessing of elastic instability. *Nano Lett.* 8, 1192–1196.
- Zhuang, Y., Chen, L., Zhu, Z., Yang, H., 2000. Preparation and separation function of N-isopropylacrylamide copolymer hydrogels. *Polym. Adv. Technol.* 11, 192–197.